On the Variation of the Effect of Natural Gas Fraction on Dual-Fuel Combustion of Diesel Engine Under Low-to-High Load Conditions

Amin Yousefi[1]*, Madjid Birouk[1] and Hongsheng Guo[2]

[1]*Department of Mechanical Engineering, University of Manitoba, Winnipeg, MB, Canada, [2]Energy, Mining and Environment Center, National Research Council Canada, Ottawa, ON, Canada*

Natural gas–diesel dual fuel (NDDF) engine has the potential to significantly reduce carbon dioxide (CO_2) and particulate matter (PM) emissions while retaining the diesel engine's high efficiency and reliability. The operation and performance of the NDDF engine depend on natural gas energy fraction (%NG), which ranges from low %NG, where diesel fuel provides most of the combustion energy, to high %NG, where diesel fuel is used only to initiate combustion. Although pertaining published studies demonstrated that the effect of %NG on the combustion performance and emissions of the NDDF engine depend upon the engine load, none of these studies discussed the reasons behind this dependence. The present study attempts to shed light on this issue by experimentally and numerically investigating the effect of different %NGs on the NDDF engine under different load conditions. Both experimental and numerical results revealed that the peak pressure rise rate (PPRR) first increases and then drops with increasing %NG under all load conditions. The calculated local equivalence ratio and charge temperature contours showed that increasing %NG to a certain limit increases local equivalence ratio inside the ignition kernel, which implies that more premixed natural gas–air mixture participates in reactions during the premixed combustion stage. This results in an increased flame temperature and higher PPRR right after ignition. However, increasing %NG beyond this range decreases local equivalence ratio inside the ignition kernel, which leads to lower PPRR. Increasing %NG retards the combustion phasing at low-to-medium load conditions. However, increasing %NG generally advances the combustion phasing under medium-to-high load conditions due to the fact that the flame propagation speed of natural gas–air mixture increases with %NG at medium-to-high load conditions. Methane emissions grow with increasing %NG under all examined engine

Abbreviations: %NG, %NG; AMR, adaptive mesh refinement; ATDC, after top dead center; BMEP, break mean effective pressure; BTE, brake thermal efficiency; CA10, crank angle of 10% heat release; CA50, crank angle of 50% heat release; CA90, crank angle of 90% heat release; CAD, crank angle degree; CFD, computational fluid dynamics; CO, carbon monoxide; CO_2, carbon dioxide; COV, coefficient of variation; EGR, exhaust gas recirculation; EVC, exhaust valve closing; EVO, exhaust valve opening; GHG, greenhouse gas; HRR, heat release rate; IMEP, indicated mean effective pressure; ITE, indicated thermal efficiency; IVC, intake valve closing; IVO, intake valve opening; LHV, lower heating value; NDDF, natural gas/diesel dual-fuel; NOx, nitrogen oxides; PM, particulate matter; PPRR, peak pressure rise rate; RPM, revolution per minute; SODI, start of diesel injection; UHC, unburned hydrocarbon.

load conditions. However, this growth becomes much smaller under medium-to-high engine load conditions. Increasing %NG significantly increases greenhouse gas (GHG) emissions under lower load conditions. However, using advanced diesel injection timing decreases GHG emissions of the NDDF engine under lower load conditions. Increasing % NG decreases GHG emissions by 6%–11% under medium-to-high load conditions.

INTRODUCTION

Diesel engines have been widely used in many engineering applications such as in transportation and stationary power generation industries due to their higher fuel efficiency and reliability as compared with the spark ignition engines. However, high levels of carbon dioxide (CO_2), nitrogen oxides (NO_x), and particulate matter (PM) emissions are becoming serious problems for the future of conventional diesel engines. In recent years, increased fuel cost and alarming environmental issues have forced the governing bodies of developed countries to implement stringent regulations to lower greenhouse gas (GHG) and pollutant emissions. For example, the Government of Canada has set a new target to reduce GHG emissions by 30% and 80% below the 2005–2006 levels by 2030 and 2050, respectively (Treasury Board of Canada Secretariat" 2017). This has exerted a significant pressure on industries using diesel engines, such as transportation and power generation. Therefore, greater research focus is placed on developing more efficient and greener power generation systems with the aim to alleviate dependency on fossil fuels and abate harmful emissions. Electrification has recently drawn great attention in automotive applications. However, its widespread adoption, especially in the heavy-duty engine market, is still impeded by several problems that include charging time, energy density, cost of materials, durability, and reliability (Guo and Liko, 2019). Therefore, a heavy-duty diesel engine will continue to predominate in private and public transportation at least for the next two to 3 decades (Bataille et al., 2015).

Efficiency improvement and fuel switching play an important role in emission reduction of heavy-duty diesel engines (Yousefi et al., 2015; Yousefi and Birouk, 2016). Natural gas is a promising fuel for transportation owing to its abundance, low carbon, and superior combustion characteristics. Combustion of natural gas reduces CO_2 emissions by up to ~20–30% (or up to ~80–90% with renewable natural gas) and produces lower PM emissions than does diesel (Yousefi et al., 2017; Guo and Liko, 2019). Therefore, replacing diesel fuel by natural gas can substantially reduce CO_2 and PM emissions. Natural gas–diesel dual fuel (NDDF) engine has emerged as a practical and efficient technology to satisfy increasingly stringent emission regulations in the near future (Rochussen and Kirchen, 2018; Yousefi et al., 2018). In the NDDF engine, the premixed natural gas–air mixture is compressed during the compression stroke and then auto-ignites upon the injection of diesel fuel. The NDDF engine can achieve similar (or sometimes higher) thermal efficiency than the diesel engine can (Yousefi and Birouk, 2017; Ahmad et al., 2018; Zheng et al., 2019). The NDDF engine can also be reverted back to diesel operation in the case of intermittent natural gas supply. The

main problem of NDDF engine technology is high unburned methane (CH_4) emissions under low-to-medium engine load conditions due to poor flame propagation under lean premixed natural gas–air mixture conditions (Jiaqiang et al., 2018; Shim et al., 2018). It is reported that CH_4 has a global warming potential of ~20–30 times more than CO_2 over a 100-year period (Yousefi et al., 2019) and, therefore, is a critical exhaust species to minimize.

The operation of the NDDF engine is governed by natural gas substitution ratio or natural gas energy fraction, which is defined as the energy content of natural gas divided by the total energy content of both natural gas and diesel fuel. This ranges from lower addition of natural gas, where the diesel fuel shoulders most of the combustion energy burden, to high substitution ratio where natural gas is the main fuel and diesel is used primarily as an ignition source. The operation of the NDDF engine under different %NGs has several strengths and drawbacks. While lower %NG is beneficial for obtaining dual-fuel engine without a costly engine retuning, higher natural gas usage is favored in order to reduce fuel cost and more importantly to reduce GHG and other pollutant emissions. The latter option may need significant engine functional alterations to meet operational and emission standards.

The effect of %NG on the combustion characteristics of the NDDF engine under different load and speed conditions has been extensively studied (e.g., Papagiannakis and Hountalas, 2004; Dahodwala et al., 2014; Lounici et al., 2014; Tablan 2014; Cesar et al., 2015; Guo et al., 2015; Nithyanandan et al., 2016; Guo et al., 2017; Mattson et al., 2018; Song et al., 2018; Guo and Liko, 2019). For instance, Papagiannakis and Hountalas (2004) compared the combustion characteristics of the NDDF engine (%NG = 84%) with those of its diesel engine counterpart at different load conditions. They found that the NDDF engine features longer ignition delay than does the diesel engine at low-to-high load conditions. They also noted that the combustion duration of the NDDF engine is longer than that of the diesel engine at low-to-medium load conditions. However, with the increase of engine load, the combustion duration of NDDF becomes shorter than that of the diesel engine especially at low engine speeds (Papagiannakis and Hountalas, 2004). Lounici et al. (2014) found that the NDDF engine has slightly more retarded start of combustion than has the diesel combustion mode at low-to-high load conditions. They also revealed that the peak pressure of the NDDF engine is lower at low-to-medium load conditions. However, at higher engine loads (e.g., over 50%), the peak pressure and heat release rate (HRR) of the NDDF engine are found higher than those of the diesel engine (Lounici et al., 2014). Cesar et al. (2015) reported similar observations. (Guo et al., 2015; Guo et al., 2017; Guo and Liko, 2019) examined the effect of different natural energy fractions on

the combustion performance and emissions of the NDDF engine at low-to-high load conditions. They showed that increasing %NG retards the combustion phasing and decreases the brake thermal efficiency (BTE) under low-to-medium engine load conditions. However, they found that increasing %NG advances the combustion phasing and increases the BTE at medium-to-high engine load conditions. Nithyanandan et al., (2016) studied the effect of %NG on the NDDF engine at medium-to-high load conditions. They found that peak pressure increases with %NG up to 70% and then declines afterwards. They also observed that the ignition delay progressively increases, whereas the combustion duration becomes shorter up to 70% %NG and then starts increasing with further increase in natural gas substitution (Nithyanandan et al., 2016). Matteson et al. (Mattson et al., 2018) studied the effect of different %NG on the combustion characteristics of the NDDF engine under four different engine load conditions. They showed that, at low-to-medium engine load conditions, increasing %NG decreases the peak pressure and retards the combustion phasing. They reported, however, that increasing %NG up to 60% advances the combustion phasing at medium-to-high load conditions, while further increase in the %NG retards the combustion phasing (Mattson et al., 2018). They concluded that, at low %NG (i.e., 0–18%), the combustion generally mimics that of diesel where, for example, the ignition delay remains unchanged and the unburned hydrocarbon (UHC) emissions worsen under all engine load conditions. They also found that midrange natural gas substitution ratio (40–60%) increases the engine thermal efficiency at medium-to-high load conditions (Mattson et al., 2018).

The briefly reviewed literature above showed that the effect of %NG on the combustion performance (e.g., combustion phasing and efficiency) and emissions of the NDDF engine greatly depends upon the engine load. However, none of these studies discussed the reasons behind this dependence on the engine load. The present study is an attempt to shed light on this issue by experimentally investigating the effect of different %NGs on the NDDF engine under different load conditions [brake mean effective pressures (BMEPs) of 4.05, 8.10, 12.15, and 17.60 bar] including testing at different %NGs (i.e., 0%–90%) in order to comprehensively investigate the different phenomena observed at each operational regime. Measured cylinder pressure, HRR, combustion timings, thermal efficiency, and engine out emissions (i.e., methane and CO_2 equivalent) are also considered. Moreover, a computational fluid dynamics (CFD) model based on CONVERGE 2.4 software is developed to help understand the experimental observations in the engine combustion chamber. Specifically, local equivalence ratio, cylinder charge temperature, size of ignition kernels, and flame propagation speed during premixed combustion and flame propagation stages are all investigated to aid in interpreting the experimental observations.

EXPERIMENTAL SETUP AND CONDITIONS

A brief summary of the engine test setup is presented here since more detailed description is reported elsewhere (Guo et al., 2015; Guo et al., 2017; Yousefi et al., 2017). **Figure 1** shows a schematic of the experimental setup, and **Table 1** lists the basic engine specifications. Experiments were conducted using a modified single cylinder Caterpillar's 3400-series heavy-duty diesel engine. The engine was equipped with a high-pressure common-rail direct diesel injection system. The diesel fuel injection was controlled using a data acquisition hardware (National Instruments, model PXI-1031chassis) and LabVIEW-based software (Drivven, Inc.). A natural gas injector manufactured by Alternative Fuel Systems, Inc. (Calgary, Alberta, Canada) was mounted on the intake manifold to create the premixed charge of natural gas–air mixture. The quantity of diesel and natural gas mass flows were measured by Bronkhorst mass flowmeters. Intake and exhaust surge tanks were used to reduce pressure pulsation and simulate the turbocharging system. The intake air mass flow was measured by a turbine mass flow meter.

Natural gas energy fraction is calculated and calibrated by the mass flow rates and lower heating values of diesel and natural gas.

$$\%NG = \frac{\dot{m}_{NG}LHV_{NG}}{\dot{m}_{NG}LHV_{NG} + \dot{m}_{D}LHV_{D}} \tag{1}$$

where $\dot{m}$ represents mass flow rate and LHV represents low heating value. Subscripts NG and D represent natural gas and diesel, respectively.

The engine speed and load were controlled by the engine's electronic control module and an AVL Digalog Testmate. Cylinder pressure was captured by a water-cooled pressure transducer (Kistler model 6041A) coupled with an AVL real-time combustion analysis system, which samples 100 consecutive cycles with a resolution of 0.2 crank angle degree (CAD). California Analytical Instruments' series 600 gas analyzer was used to measure CO_2, carbon monoxide (CO), NO_x, and CH_4 emissions. Soot measurement was performed by an AVL smoke meter (415S).

A maximum peak pressure rise rate (PPRR) of 13 bar/CAD, a maximum cylinder pressure of 150 MPa, and a coefficient of variation of indicated mean effective pressure (IMEP) (COV_{IMEP}) of 5% were used as the engine operating limits during testing. Experiments were carried out at four different engine load conditions including low-to-medium load (BMEPs = 4.05 and 8.10 bar) and medium-to-high load (BMEPs = 12.15 and 17.60 bar). A sweep of %NG and diesel injection timing tests were conducted when investigating each case. For all cases, the intake temperature and diesel injection rail pressure were kept constant at 40°C and 525 bar during the experiments. Exhaust gas recirculation (EGR) was not used in this study. **Tables 2, 3** give the varied and fixed experimental test conditions, respectively. It can be observed, from **Table 2**, that increasing natural gas energy fraction slightly reduces the air mass flow rate at each engine load condition. However, this does not significantly change the density of air at the timing of diesel injection since the density of air is mainly affected by the intake pressure and temperature. Testing was accomplished at steady-state conditions when the engine oil and exhaust gas temperature varied by less than 1% over a 180-s period. Engine performance data, particularly the flow rates of both gaseous and liquid fuels and engine out emissions, were collected over the course of 180 s.
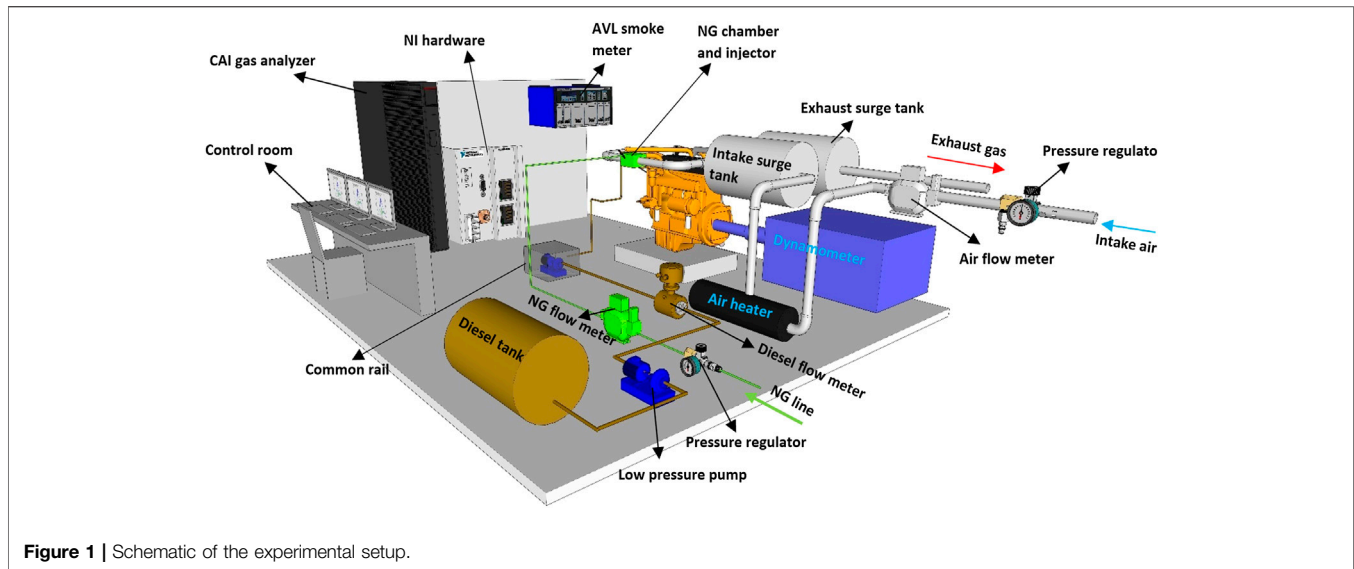
Figure 1 | Schematic of the experimental setup.

NUMERICAL MODELING AND VALIDATION

A three-dimensional model was built in CONVERGE 2.4 software (Richards et al., 2017), which is a CFD solver for modeling complex geometries and complicated phenomena such as engine combustion. Details of the developed CFD model can be found in Yousefi et al. (Yousefi et al., 2018; Yousefi et al., 2019). A transient chemistry solver, named as SAGE (Richards et al., 2017), was used to implement the chemistry calculation. SAGE calculates the reaction rates for each elementary reaction, while the CFD solver solves the governing transport equations. Diesel fuel was represented by n-heptane, and natural gas oxidation was represented by methane in the reaction mechanism that consisted of 76 species and 464 reactions (Rahimi et al., 2010). This

mechanism, which was validated under different natural gas/diesel dual-fuel engine operating conditions, has also been adopted by CONVERGE software for NDDF combustion simulation (Richards et al., 2017). Kelvin Helmholtz–Rayleigh Taylor and O'Rourke models were applied to model the diesel spray breakup process and droplet collision, respectively (Senecal et al., 2007).

The simulation started from the intake valve closing (IVC) and terminated at the exhaust valve opening (EVO). Since the test engine is a heavy-duty engine, there is a low swirl ratio at IVC, which is estimated to be 0.5. As the diesel injector was located in the central axis of the cylinder and the six nozzle holes were distributed symmetrically, only 1/6th of the combustion chamber was simulated. The baseline grid size was set to be 2 mm, and an adaptive mesh refinement (AMR) was then employed on the velocity and temperature gradients with a maximum embedding level of 3. **Figure 2** displays the piston bowl, squish dimensions, and grid refinements using CONVERGE AMR tool. The upper limit of the total cells in the computational domain is two million. The AMR enables the simulation to efficiently resolve details in the regions of the turbulent flame front and higher species concentration gradients (fine enough cell sizes of 0.25–0.5 mm), while a relatively coarse mesh was used in regions where no reactions or spray dispersion occur (Wijeyakulasuriya 2015; Jupudi et al., 2016).

The simulated pressure and HRR of different cases [under different loads, %NGs, and start of diesel injection (SODI)] are validated against the experimental data and presented in **Figure 3A–C**. Further validation cases can be found elsewhere (Yousefi et al., 2018; Yousefi et al., 2019). It can be observed that, in all these cases, the simulated and experimental pressures and HRR are in agreement. Moreover, it is observed that the agreement between the measured and simulated results of combustion characteristics (e.g., CA10-90 and CA50), thermal efficiency, and emissions is also satisfactory (all these results are presented in Section Result and Discussion).

TABLE 1 | Engine specifications.

Engine type	Single cylinder-caterpillar 3,400
Bore × stroke	137.2 mm × 165.1 mm
Conn. rod length	261.62 mm
Displacement vol.	2.44 L
Compression ratio	16.25
Diesel fuel injector-type	Common rail injector-direct injection
Number of nozzle hole	6
Nozzle hole diameter	0.23 mm
Spray umbrella angle	130°
Natural gas injection timing	−355° ATDC
Number of intake valve	2
Number of exhaust valve	2
IVO	−358.3° ATDC
IVC	−169.7° ATDC
EVO	145.3° ATDC
EVC	348.3° ATDC

ATDC, after top dead center; EVO, exhaust valve opening; EVC, exhaust valve closing; IVO, intake valve opening.

TABLE 2 | Varied experimental test conditions.

Engine load	NG (%)	Air flow (kg/h)	Diesel flow (kg/h)	NG flow (kg/h)	Diesel injection timing (ATDC)
25% load (BMEP = 4.05 bar)	0	66.89–68.82	1.79–1.91	0	−10 to −22
	25	67.53–68.13	1.31–1.40	0.41–0.44	−10 to −19
	50	66.87–68.01	0.89–0.97	0.85–0.94	−10 to −17
	75	66.59–67.69	0.42–0.50	1.24–1.47	−10 to −26
50% load (BMEP = 8.10 bar)	0	90.27–92.53	3.08–3.20	0	−14 to −28
	50	88.91–90.06	1.50–1.63	1.41–1.51	−14 to −26
	75	88.73–89.52	0.74–0.78	2.09–2.26	−14 to −25
	90	87.06–90.02	0.30–0.31	2.49–2.73	−14 to −26.5
75% load (BMEP = 12.15 bar)	0	111.93–112.45	4.50–4.73	0	−14 to −25
	25	109.81–110.82	3.26–3.64	1.01–1.12	−10 to −22
	75	108.19–106.48	1.09–1.13	3.05–3.15	−12 to −16
	90	107.27–107.92	0.42–0.48	3.69–3.83	−10.5 to −15
100% load (BMEP = 17.6 bar)	0	192.85–192.91	7.92–8.13	0	−20 to −22.5
	25	190.12–190.83	5.93–6.19	1.84–1.92	−17 to −20
	50	188.69–189.53	3.91–4.16	3.64–3.83	−14.5 to −18
	65	187.67–188.27	2.71–2.85	4.67–4.92	−12 to −16

ATDC, after top dead center; BMEP, brake mean effective pressure.

RESULTS AND DISCUSSION

In addition to the experimental data, numerical simulation results (i.e., local equivalence ratio, temperature, and CH_4 distribution contours) are also presented for some cases to help better understand the combustion process. Note that CA10, CA50, and CA90 refer to the crank angle position, which corresponds to 10%, 50%, and 90% of cumulative heat release, respectively. The CA50 and the interval from CA10 to CA90 are defined as the combustion phasing and combustion duration, respectively. The average cylinder pressure of 100 consecutive cycles is used as a primary input for calculating HRR using **Eq. 2**.

$$HRR = \frac{\gamma}{\gamma - 1} P \frac{dV}{d\theta} + \frac{1}{\gamma - 1} V \frac{dP}{d\theta} \qquad (2)$$

where γ is the ratio of specific heat at constant pressure to that at constant volume, P is the measured cylinder pressure, V is the cylinder volume, and θ is the crank angle in degrees.

Figure 4 presents the measured cylinder pressure and HRR traces for different %NGs at BMEPs of 4.05 bar (**Figure 4A**) and 12.15 bar (**Figure 4B**). For brevity, the cylinder pressure and HRR plots shown herein are only taken for the test case of SODI = −14° after top dead center (ATDC) at BMEPs of 4.05 bar (**Figure 4A**) and 12.15 bar (**Figure 4B**). It can be observed, from **Figure 4A**, that increasing %NG from 0% to 50% yields a consistent growth in the HRR peak at BMEP = 4.05 bar. This is attributed to the fact that more premixed natural gas–air mixture is burnt under premixed combustion regime. However, beyond this point

(i.e., 50%), peak HRR falls dramatically. The reason behind this will be explained in **Figure 5A**. The HRR profile of the NDDF engine at BMEP = 4.05 bar indicates that there are only two stages of combustion, namely, premixed followed by diffusion, similar to diesel engine. It can be seen that after premixed and diffusion combustion, there is no flame propagation of natural gas since the premixed natural gas–air mixture is very lean. **Figure 4A** also indicates that adding small amount of natural gas (e.g., 25%) yields a relatively minor change in the cylinder pressure profile, with the most significant difference being its lower cylinder peak pressure compared with 0% NG. Further increase in %NG (i.e., 50% and 75%) continuously lowers the peak cylinder pressure, indicating the struggle of the engine to combust large amount of natural gas. This is also reflected in the PPRR for 75% NG under low load conditions, as it will be discussed later (**Figure 5A**).

A different combustion behavior occurs under higher engine load conditions. As shown in **Figure 4B**, increasing %NG from 0% to 75% slightly increases the first peak of HRR similar to the case at lower engine load (**Figure 4A**). This is due to the fact that a higher portion of natural gas–air mixture participates in reactions in the premixed combustion stage when increasing %NG from 0% to 75% at BMEP = 12.15 bar. **Figure 4B** also shows that the second peak of HRR significantly increases when increasing %NG from 0% to 75%, implying a shift from diffusion to flame propagation of natural gas–air mixture combustion. It can be seen in **Figure 4B** that further increase in %NG from 75% to 90% slightly decreases the first peak while significantly decreases the

TABLE 3 | Fixed experimental test conditions.

Engine load	Intake temperature (°C)	Intake pressure (bar)	Speed (RPM)	Injection pressure (bar)	Engine oil temperature (°C)	Coolant water temperature (°C)
25% load	40	1.05	910	525	85	85
50% load	40	1.50	910	525	85	85
75% load	40	1.80	910	525	85	85
100% load	40	2.20	1,120	525	85	85
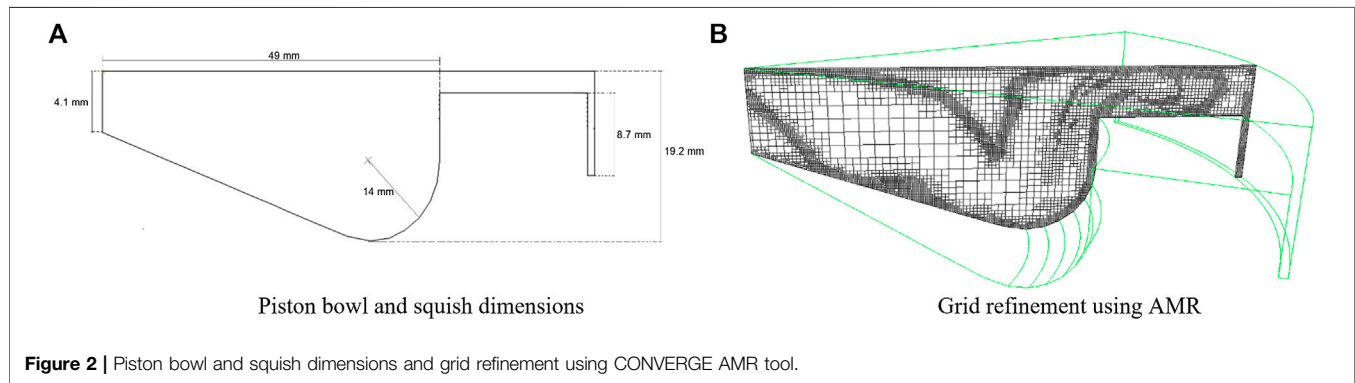
Figure 2 | Piston bowl and squish dimensions and grid refinement using CONVERGE AMR tool.

second peak of the HRR profile. The former is attributed to the fact that the overall equivalence ratio in the flame kernel in the premixed combustion becomes lower, and the latter is due to lower flame propagation speed of natural gas–air mixture. Further related discussion is provided later on. The cylinder pressure profile (**Figure 4B**) indicates that the addition of a small amount of natural gas (i.e., 25% NG) has only a slight effect (slight increase in cylinder peak pressure) on the cylinder pressure compared with that of diesel combustion (i.e., 0% NG). However, a higher increase in %NG (i.e., 75%–90%) results in a significant increase in the peak pressure.

Figure 5 displays the measured and calculated PPRR for different %NGs and SODIs at BMEPs of 4.05 and 12.15 bar. The simulation was only conducted for one SODI at each load condition to minimize the computation cost. It can be observed from the measured results that advancing SODI increases the PPRR under all examined engine load conditions. This is mainly due to the fact that advancing SODI lengthens the ignition delay, which allows more time for diesel fuel to mix with the premixed natural gas–air mixture before the start of combustion. It is observed that PPRR jumps under advanced SODI and high % NGs of 75 and 90% at BMEP of 12.15 bar. Both measured and calculated results showed that at a given SODI, PPRR first increases and then starts declining with increasing %NG under both low and high load conditions. For example, at BMEP of 4.05 bar (**Figure 5A**), PPRR increases with increasing %NG from 0% to 50% and then drops with further increase in %NG. Also, at BMEP of 12.15 bar (**Figure 5B**), PPRR first increases with increasing %NG from 0% to 75% and then starts decreasing with further increase in %NG up to 90%. In order to understand the causes behind this behavior, the concentration contours of local equivalence ratio (at CA10), cylinder temperature (at 2° after CA10), and CH_4 (at 2° after CA10) under different %NGs and a fixed SODI of $-14°$ ATDC are presented in **Figure 6**. As shown in **Figure 6A** (BMEP = 4.05 bar), increasing %NG from 0% to 50% increases the local equivalence ratio in the ignition kernel zone. This implies that more natural gas–air mixture burns under premixed combustion stage, which results in increased temperature, intense HRR (**Figure 4A**), and higher PPRR right after the onset of ignition (**Figure 5A**). However, with further increase in %NG from 50% to 75%, the local equivalence ratio in the ignition kernel zone decreases as more lean natural gas–air mixture mixes with diesel before ignition. This results in a slower
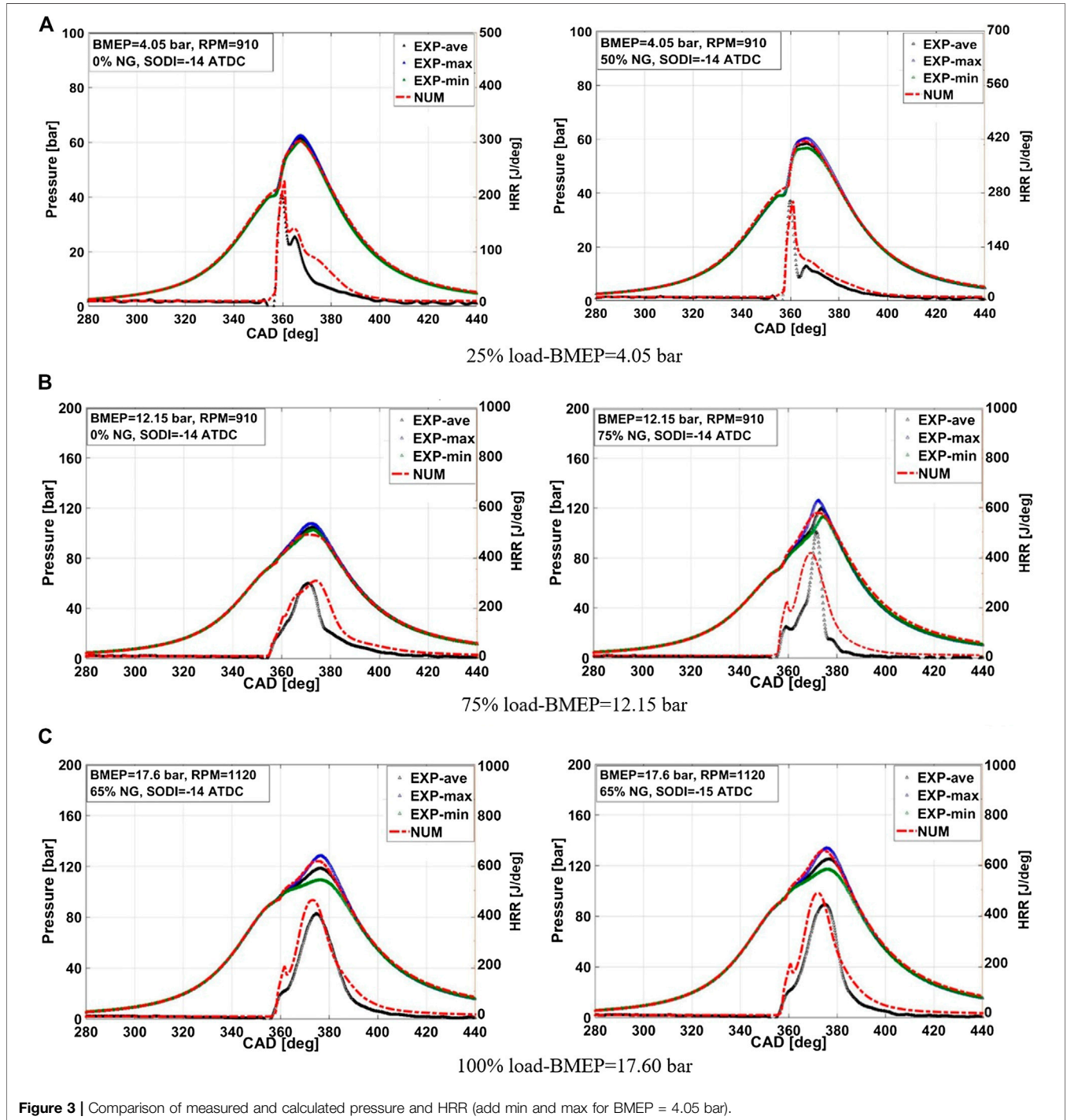
heat release and lower PPRR. A similar behavior is observed under higher engine load conditions (at BMEP of 12.15 bar) (**Figure 6B**).
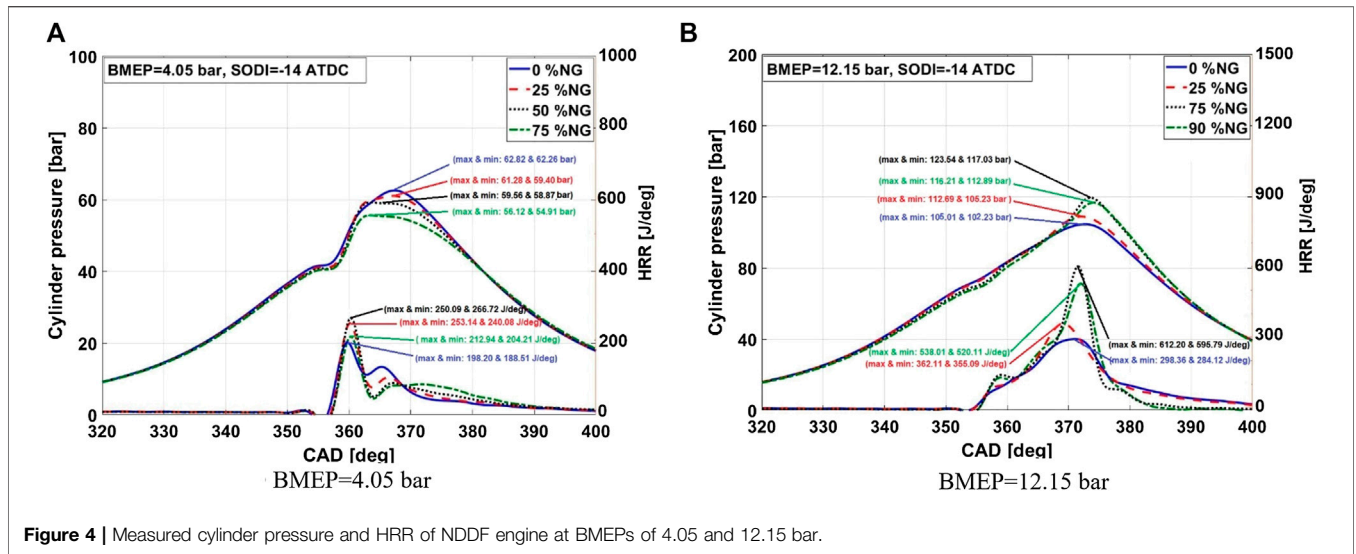
Figure 7 shows the variation of combustion phasing (CA50) at four different engine load conditions. It can be seen that advancing diesel injection timing (in the range of conventional diesel engine) advances the combustion phasing of the NDDF engine at all load conditions. This is expected since diesel and natural gas–air mixture starts mixing earlier with advancing diesel injection timing. At a given SODI, the effect of %NG on combustion phasing varies with the engine load. Under BMEPs of 4.05 and 8.10 bar (**Figure 7A,B**), increasing %NG retards the combustion phasing. However, at BMEPs of 12.15 and 17.60 bar (**Figure 7C,D**), the combustion phasing generally advances when increasing %NG except in the case when increasing natural gas fraction from 75% to 90% at BMEP of 12.15 bar where the combustion phasing slightly retards. To understand the reason behind this observation, the temperature distribution contours under BMEPs of 4.05 and 12.15 are presented in **Figure 8A,B**, respectively.

As previously mentioned, increasing %NG from 0% to 50% increases the local equivalence ratio, whereas further increase up to 75% decreases the local equivalence ratio in the ignition kernel zone at the onset of combustion under BMEP = 4.05 bar. After the premixed combustion stage, the equivalence ratio of natural gas–air mixture around the ignition kernel zone (**Figure 6A**) is very low and hence cannot sustain further burning of the mixture. In addition, the temperature inside the combustion chamber (**Figure 8A**) is not high enough to support the burning of the remainder of the mixture. For example, for 50% NG, the local equivalence ratio and temperature of natural gas–air mixture surrounding the ignited zone is approximately 0.25 and 1,000°C at an engine crank angle of CA10. Increasing %NG to 75% slightly increases the local equivalence ratio around the ignition pocket ($\phi \cong 0.34$), while the temperature in the flame kernels drops as shown in **Figure 8A**. These conditions in the cylinder make it more difficult for the pilot diesel to completely combust the premixed natural gas–air mixture, and hence, the flame quenches after the elapse of the premixed and diffusion combustion stages. Therefore, more heat is released at a crank angle farther away from the TDC, which causes combustion phasing to retard when increasing %NG from 0% to 75% at BMEP = 4.05 bar.

However, increasing %NG, generally, advances the combustion phasing under BMEPs of 12.15 and 17.60 bar. **Figure 8B** shows the high temperature regions inside the combustion chamber. The expansion of high temperature zone at a specific duration of the engine crank angle after the elapse of diffusion combustion is a result of flame propagation of the premixed natural gas–air mixture. Hence, temperature distribution will be used here as a representation of flame propagation to qualitatively compare the results at different % NGs. As shown in **Figure 8B**, at 25% NG, a high temperature region occurs only in the central region of the combustion chamber where the local equivalence ratio is also high. However, the flame does not propagate into the regions near the cylinder wall and squish regions. This is due mainly to the low equivalence ratio around the ignition pocket (**Figure 6B**). With further increase in %NG to 75%, the high temperature zone

Figure 3 | Comparison of measured and calculated pressure and HRR (add min and max for BMEP = 4.05 bar).

Figure 4 | Measured cylinder pressure and HRR of NDDF engine at BMEPs of 4.05 and 12.15 bar.

occupies almost the entire combustion chamber (i.e., piston bowl, wall, and squish regions at engine crank angle of 12° after CA10) within the same crank angle duration (from 4° to 12° after CA10) similar to the case of 25% NG. This is an indication of higher flame propagation speed of natural gas–air mixture. Under this condition, both the equivalence ratio of the premixed natural gas–air mixture ($\phi_{NG} \cong 0.65$) and the charge temperature (T $\cong$ 1,150°C) are higher inside the cylinder, which significantly enhance the flame propagation speed of the premixed natural gas–air mixture. With further increase in %NG to 90%, the high temperature zone (**Figure 8B**) does not completely fill the

combustion chamber at engine crank angle of 12° after CA10 compared with 75% NG. This indicates that the flame propagation speed slightly decreases compared with that of 75% NG. Under this condition (90% NG), the equivalence ratio of the premixed natural gas–air mixture is $\phi \cong 0.75$, which is higher than that of the 75% NG and is expected to improve the flame propagation speed. However, at 90% NG, the charge temperature at the beginning of the combustion is lower than that of 75% NG (shown in **Figure 6B**), which reduces the flame propagation speed of natural gas–air mixture. Moreover, it can be seen, from **Figure 6B**, that at engine crank angle of 2° after

Figure 5 | PPRR of NDDF engine at BMEPs of 4.05 and 12.15.
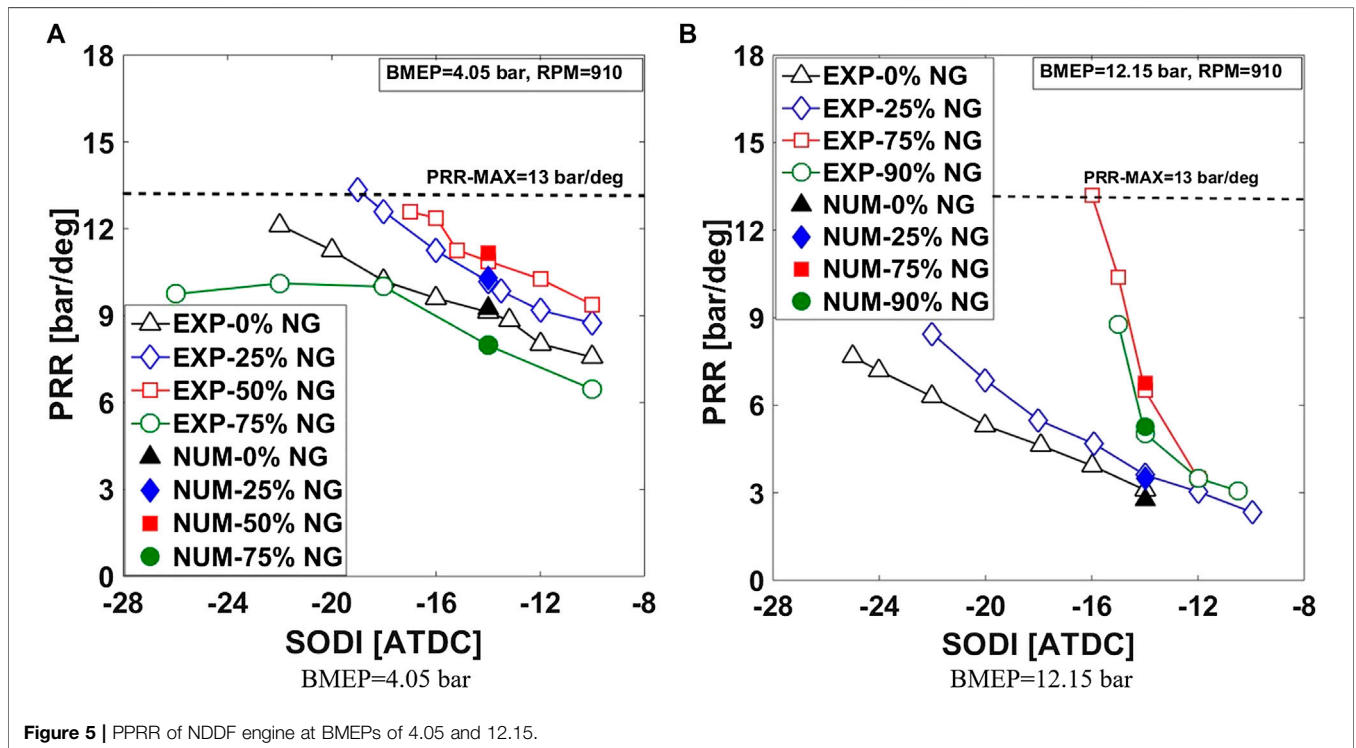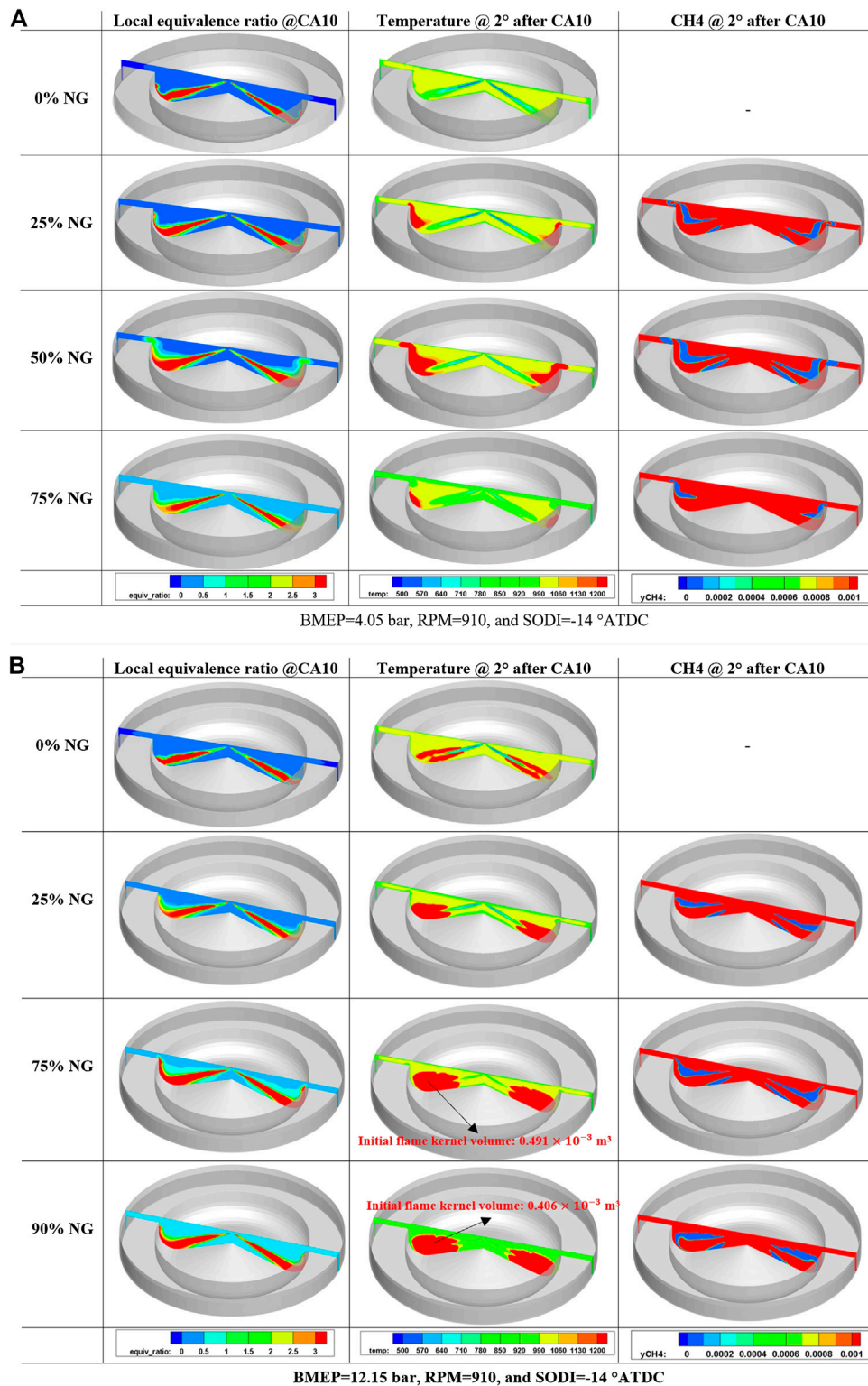
Figure 6 | Local equivalence ratio, temperature, and CH4 distributions of NDDF engine under BMEPs of 4.05 and 12.15 bar.
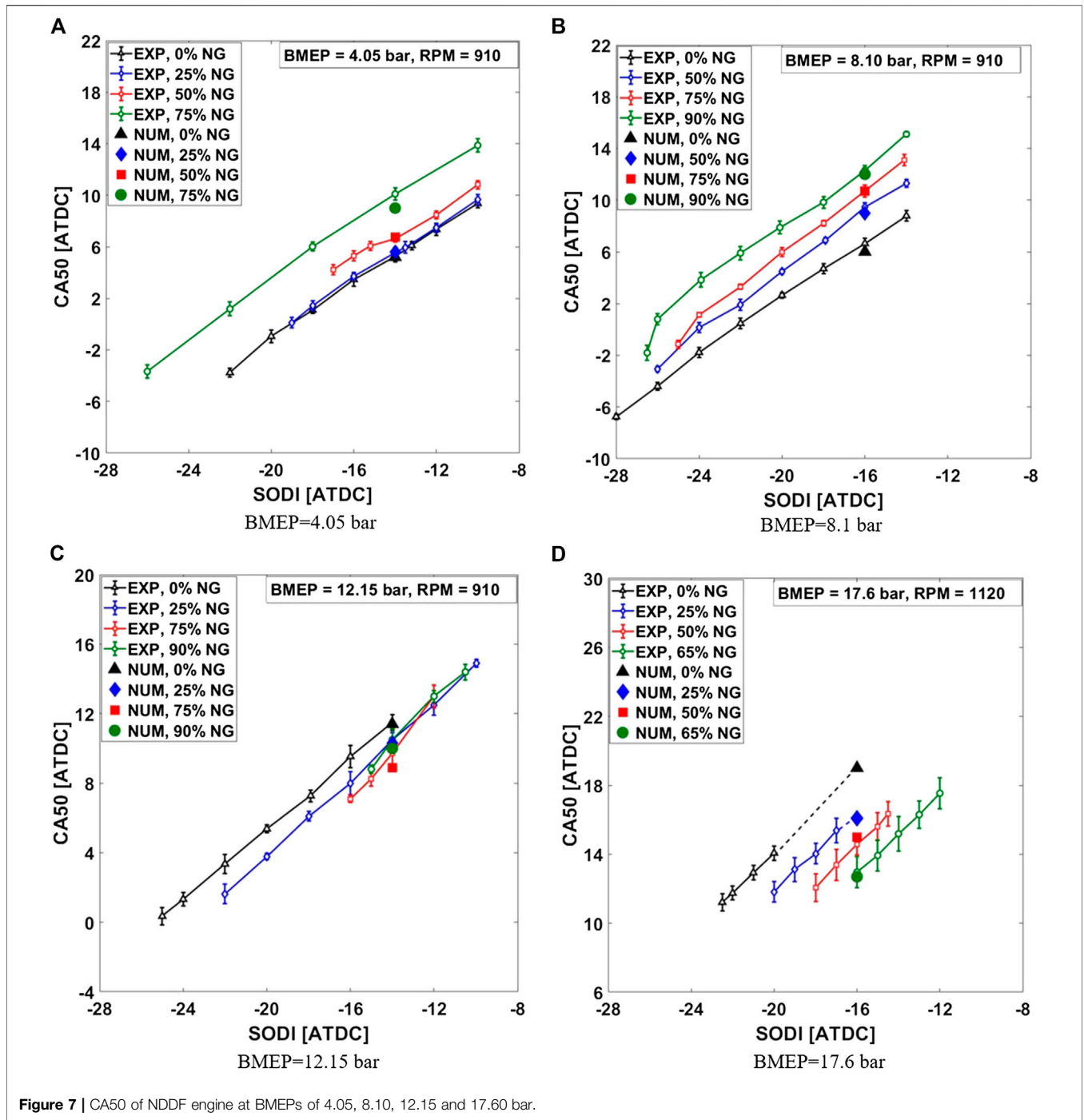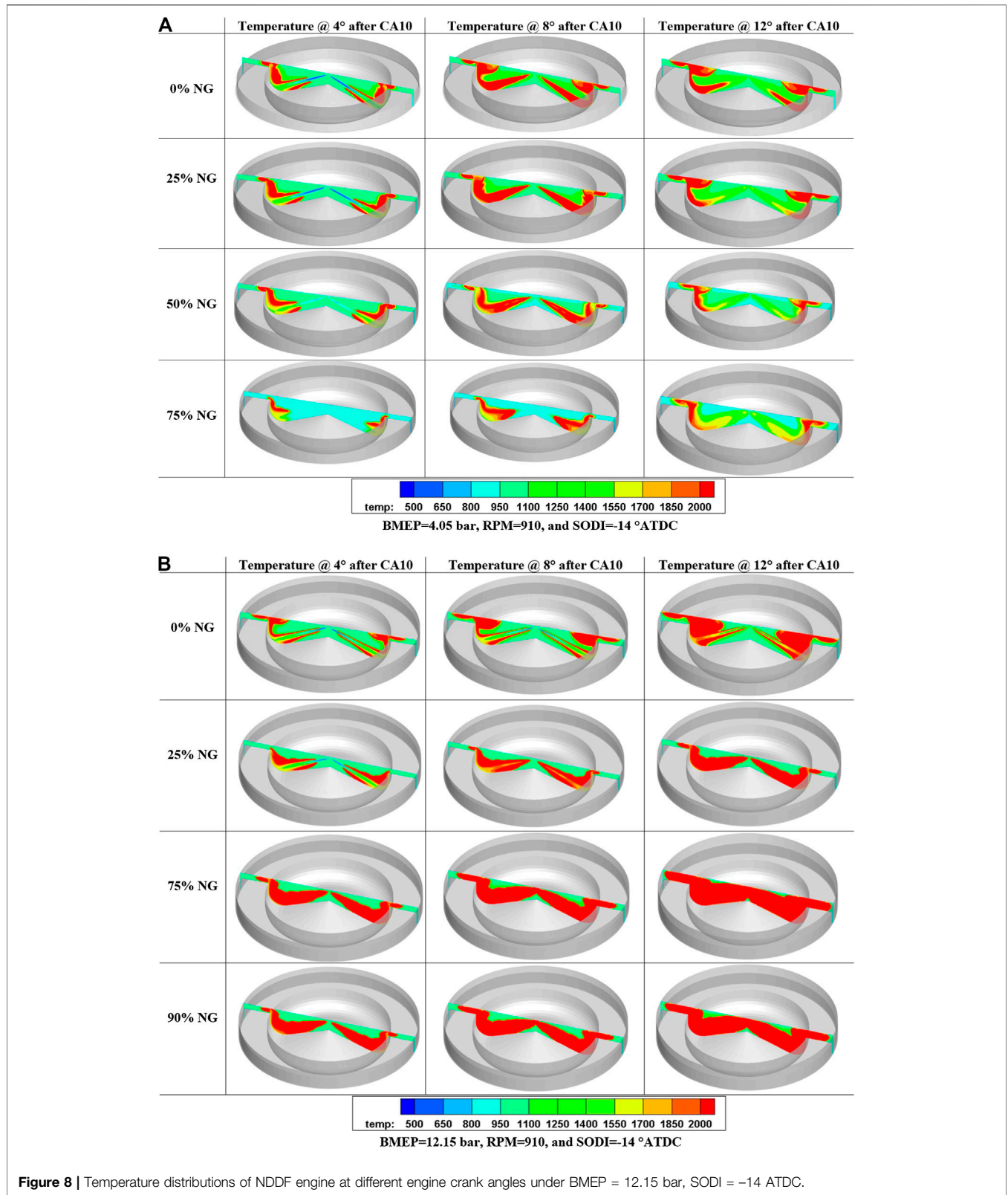
Figure 7 | CA50 of NDDF engine at BMEPs of 4.05, 8.10, 12.15 and 17.60 bar.

CA10, the size of the initial flame kernel at 90% NG (i.e., volume of initial flame kernel at 90% NG = 0.406×10^{-3} m^3) is smaller than that at 75% NG (i.e., volume of initial flame kernel at 75% NG = 0.491×10^{-3} m^3), which is due to the lower amount of injected diesel fuel (lower equivalence ratio inside the flame kernel). This could reduce the flame propagation speed of natural gas–air mixture. The effect of lower cylinder temperature and smaller initial flame kernel on flame propagation speed of natural gas–air mixture is more

significant than that of higher premixed equivalence ratio, which results in lower flame propagation speed and slightly retarded combustion phasing when %NG increases from 75% to 90%.

Figure 9 shows the combustion duration of the NDDF engine at BMEPs of 4.05 and 12.15 bar. It can be seen that the combustion duration increases with increasing natural energy fraction from 0% to 75% at BMEP of 4.05 bar (**Figure 9A**). As shown in **Figure 7**, increasing %NG retards the combustion
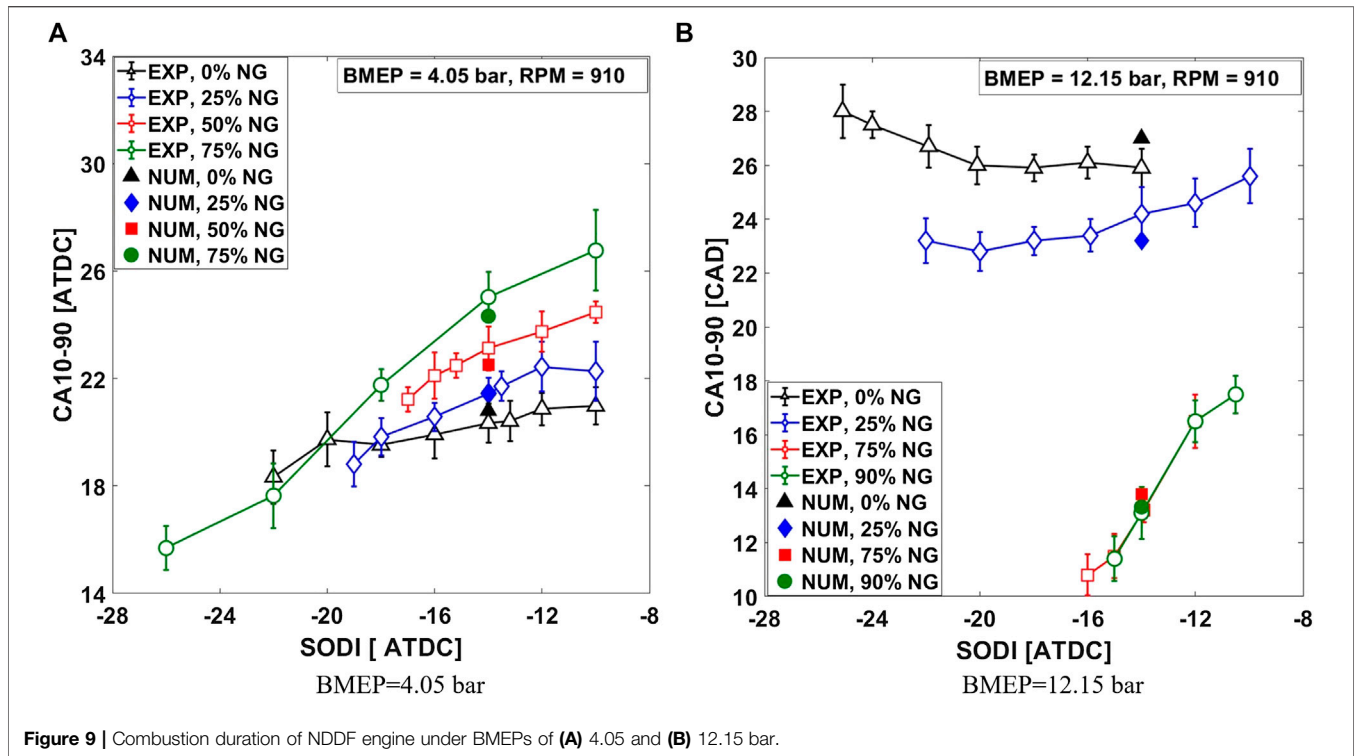
Figure 8 | Temperature distributions of NDDF engine at different engine crank angles under BMEP = 12.15 bar, SODI = −14 ATDC.

Figure 9 | Combustion duration of NDDF engine under BMEPs of **(A)** 4.05 and **(B)** 12.15 bar.

phasing and therefore lengthens the combustion duration. However, at BMEP of 12.15 bar, the combustion duration significantly decreases with increasing %NG from 0% to 75%. This is due mainly to the increase in the flame propagation speed of natural gas–air mixture as indicated by the flame temperature distribution contours in **Figure 8B**. The combustion duration slightly increases with further increase in %NG from 75% to 90%, which is due mainly to the lower charge temperature and smaller flame kernel size at the onset of combustion.

Figure 10 depicts the variation of indicated thermal efficiency (ITE) of the NDDF engine for four different load conditions. ITE is calculated as (Yousefi et al., 2019)

$$ITE = \frac{\text{Indicated power}}{(\dot{m}_{NG}LHV_{NG}) + (\dot{m}_{D}LHV_{D})} \times 100 \quad (3)$$

where $\dot{m}_{NG}$ and $\dot{m}_{D}$ are the mass flow rates of natural gas and diesel, respectively, and LHV_{NG} and LHV_{D} are the lower heating value of natural gas and diesel, respectively.

ITE shows a different behavior with %NG, diesel injection timing, and engine load. As shown in **Figure 10A**, at BMEP of 4.05 bar, increasing %NG at a retarded SODI (i.e., −14° ATDC) significantly decreases thermal efficiency. This is due to the failure of flame propagation of the premixed natural gas–air mixture, which causes a very late combustion phasing (**Figure 7A**) and consequently low thermal efficiency. However, advancing SODI significantly improves the combustion of premixed charge and increases thermal efficiency of the NDDF engine, especially at higher %NGs (i.e., 75% NG). Under BMEP = 4.05 bar and dual-fuel mode, the highest thermal efficiency (35.8%) is achieved at

75% NG and SODI = −26 ATDC, which is comparable with that of diesel engine.

A similar behavior occurs at BMEP = 8.10 bar (**Figure 10B**) where advancing SODI significantly improves the premixed natural gas–air mixture combustion and consequently increases thermal efficiency of the NDDF engine, especially at 90% NG. However, due to very advanced combustion phasing (**Figure 7B**), thermal efficiency starts dropping when SODI is earlier than −22° ATDC. At BMEP = 8.1 bar, the highest thermal efficiency in dual-fuel mode is 39.9%, which is obtained at 90% NG and SODI = −22° ATDC. However, the highest thermal efficiency of the diesel engine at similar conditions is only 38.6%.

Interestingly, at BMEPs of 12.15 and 17.60 bar (**Figure 10C,D**), increasing %NG significantly increases thermal efficiency of the NDDF engine at a given SODI. This is due mainly to a combination of advanced combustion phasing (**Figure 7C,D**), improved flame propagation speed of natural gas–air mixture, and shorter combustion duration. However, it can be observed, from **Figure 10C**, that increasing %NG from 75% to 90% slightly decreases thermal efficiency of the NDDF engine. This is due to the fact that the combustion phasing slightly retards and flame propagation speed slightly decreases. Advancing SODI significantly enhances thermal efficiency of the NDDF engine under medium-to-high load conditions. This is primarily attributed to better combustion phasing when advancing diesel injection timing. At BMEP = 12.15 bar, the highest thermal efficiency in dual-fuel mode is 41.4%, which is obtained at 25% NG and SODI = −22° ATDC. However, the highest thermal efficiency of its counterpart's diesel engine is 40.1%, which occurs at SODI = −24° ATDC. Moreover, at
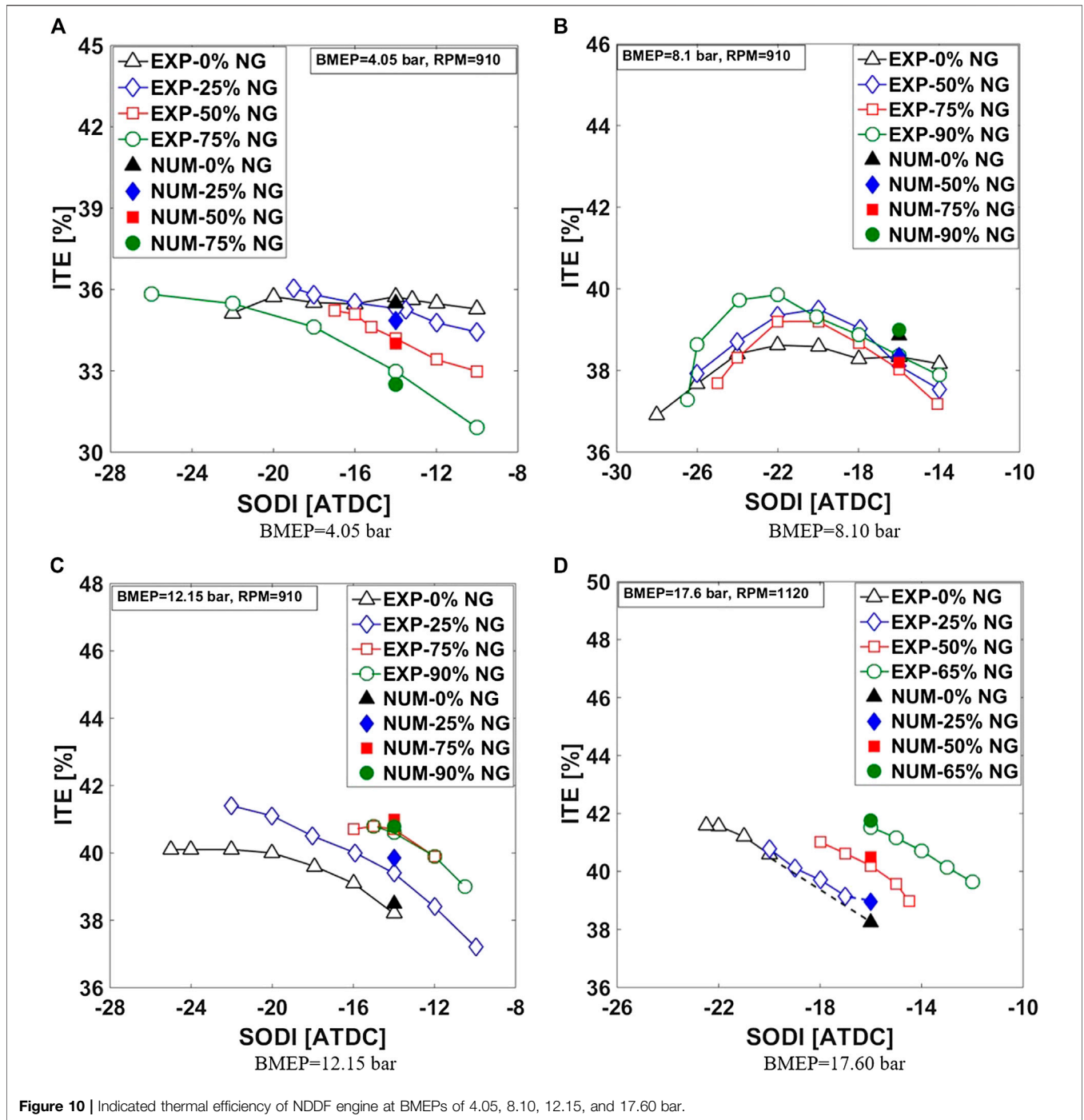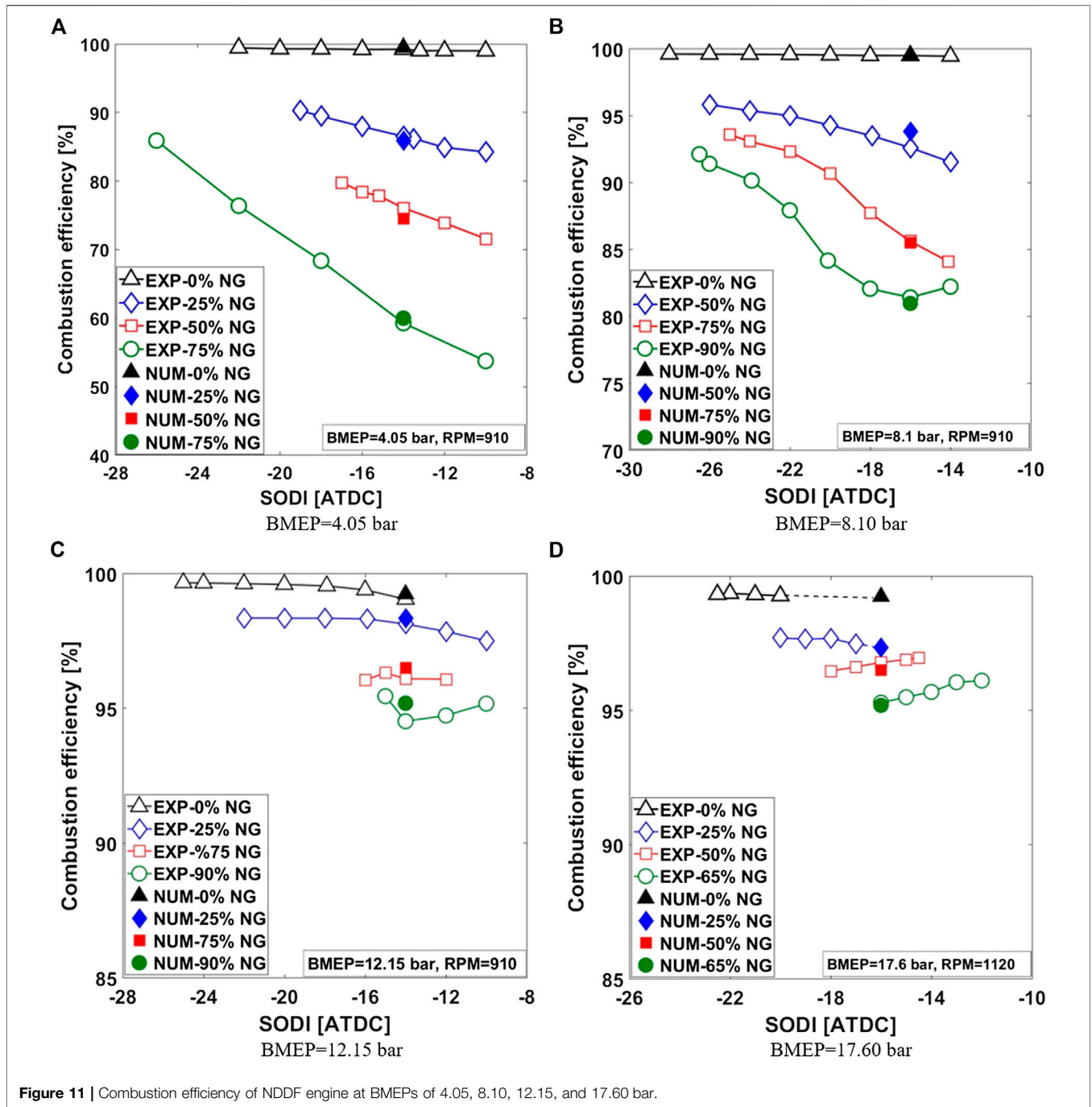
Figure 10 | Indicated thermal efficiency of NDDF engine at BMEPs of 4.05, 8.10, 12.15, and 17.60 bar.

BMEP = 17.60, the highest thermal efficiency (41.5%) of NDDF is achieved at 65% NG and SODI = −16° ATDC, which is comparable with that of the diesel (i.e., 41.6%). It can be concluded from the above discussion that, by tuning diesel injection timing and %NG, a thermal efficiency of the NDDF engine similar that of diesel can be achieved under low-to-high load conditions.

Figure 11 shows the variation of combustion efficiency of the NDDF engine at four different load conditions. Combustion efficiency is calculated using **Eq. 4**.

$$CE = \left[100 - \frac{(ISCO.LHV_{CO} + ISHC.LHV_{DF})}{(\dot{m}_{NG}.LHV_{NG} + \dot{m}_D.LHV_D)} \right]$$
$$\times\ indicated\ power \times 100 \qquad (4)$$

Figure 11 | Combustion efficiency of NDDF engine at BMEPs of 4.05, 8.10, 12.15, and 17.60 bar.

where ISCO and ISHC are, respectively, the indicated specific CO emissions and indicated specific UHC emissions (methane and non-methane emissions). LHV_{DF} is the lower heating value of dual-fuel mode, which is calculated using **Eq. 5**.

$$LHV_{DF} \; = \; \frac{\dot{m}_{NG}LHV_{NG} + \dot{m}_D LHV_D}{\dot{m}_{NG} + \dot{m}_D} \qquad (5)$$

As shown in **Figure 11**, combustion efficiency decreases with increasing natural gas energy fraction under all examined (low-to-

high) load conditions. This is mainly due to the higher amount of unburned fuel in the exhaust, which is caused by the increase in natural gas energy fraction. It can be observed in **Figures 11C,D** that at medium-to-high engine load conditions, combustion efficiency is relatively high and reaches 95% even for high natural gas energy fractions (i.e., NG = 90%). This is mainly due to improved flame propagation speed of premixed natural gas–air mixture under medium-to-high load conditions (shown in **Figure 8B**). It can be seen in **Figure 11A,B** that a decrease in combustion efficiency is more significant under low-to-medium
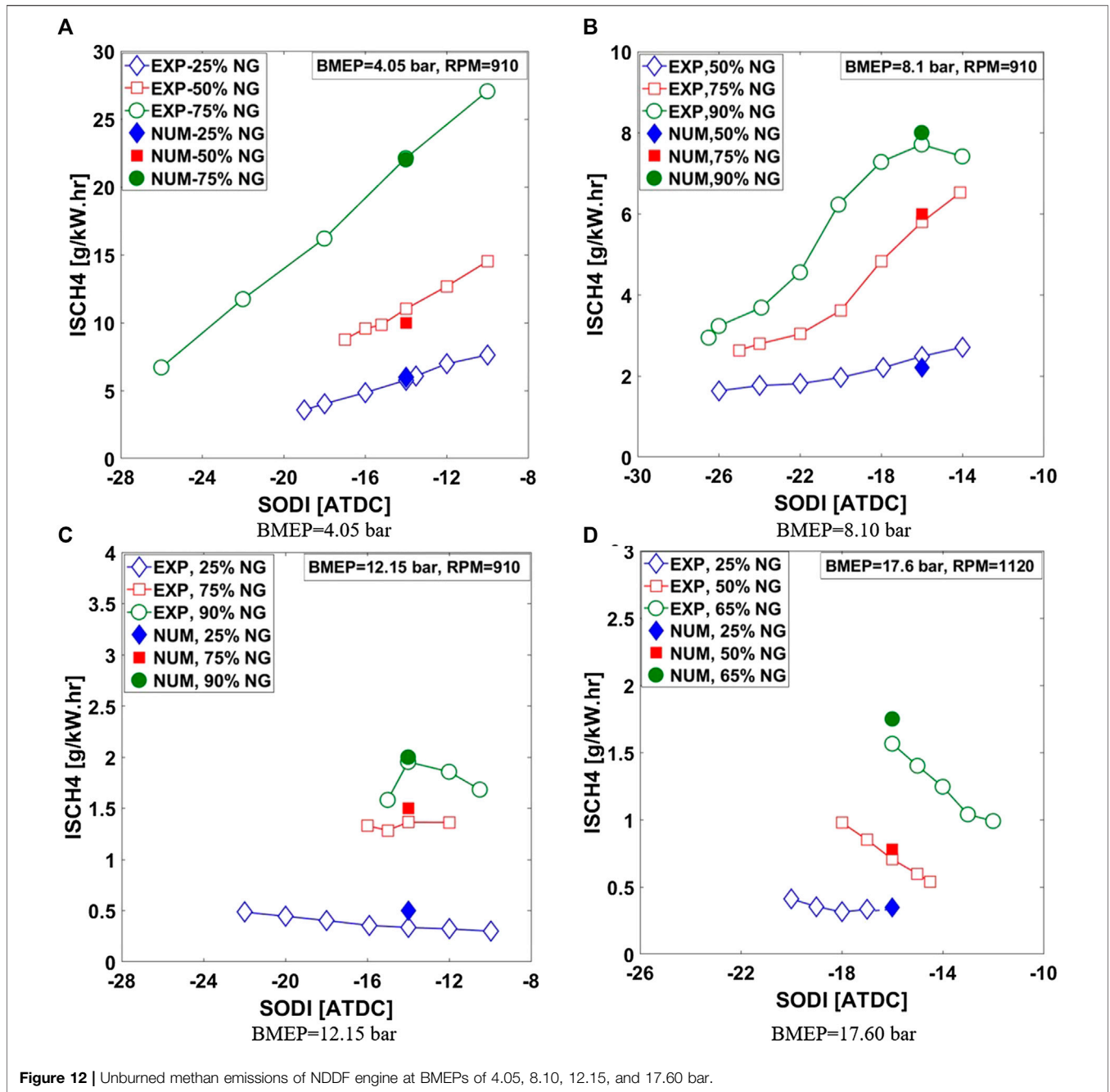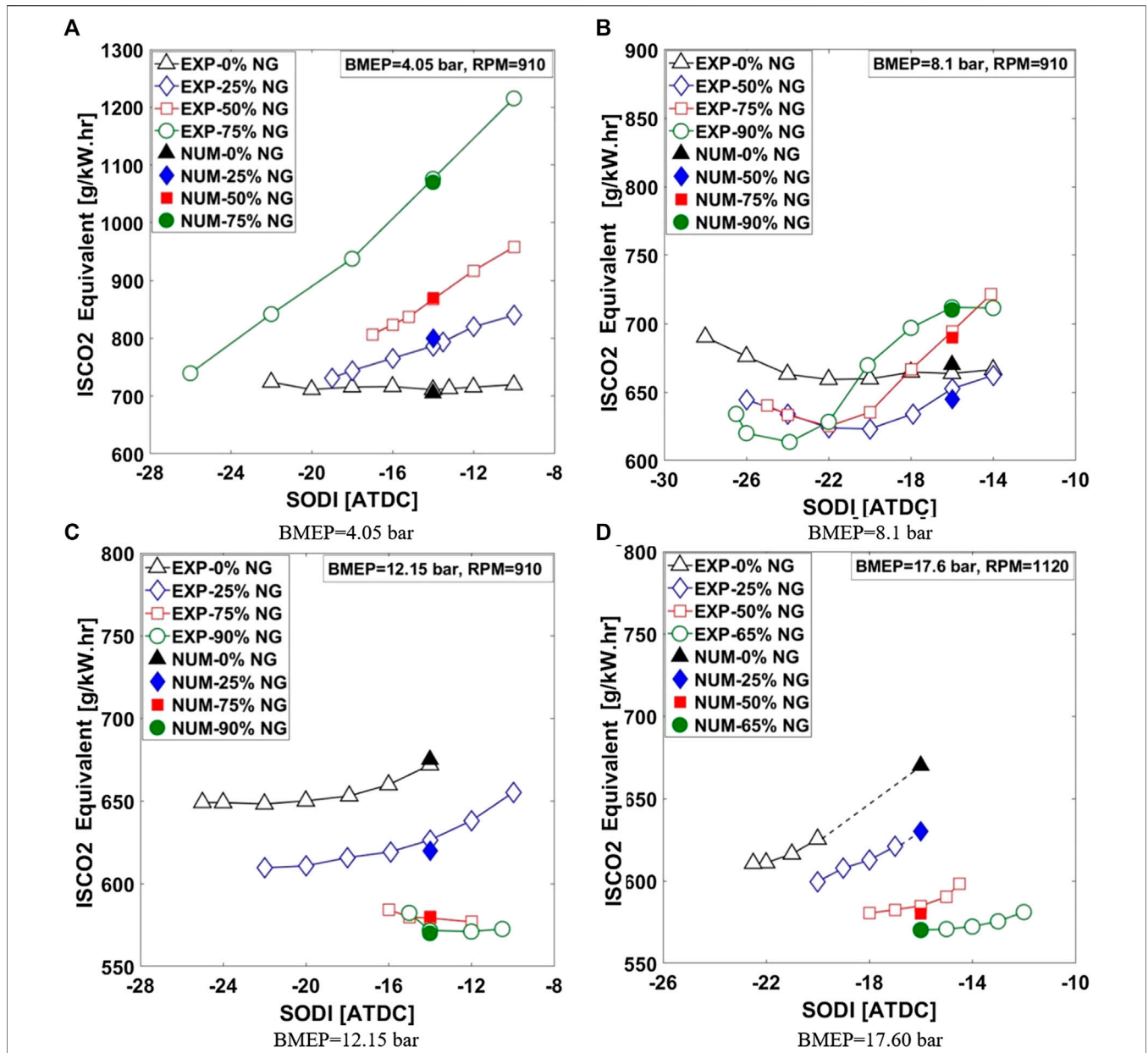
Figure 12 | Unburned methan emissions of NDDF engine at BMEPs of 4.05, 8.10, 12.15, and 17.60 bar.

load conditions, which is due to unsuccessful flame propagation of premixed natural gas–air mixture. However, advancing SODI under low-to-medium load conditions significantly improves combustion efficiency especially at higher natural gas energy fractions. This is due to the fact that advancing SODI allows more time for diesel fuel to mix with premixed natural gas–air mixture before the start of combustion, which results in improved combustion efficiency. However, advancing SODI does not significantly improve combustion efficiency of the NDDF engine at medium-to-high load conditions. This is attributed to a slight increase in unburned methane emissions when advancing

SODI under medium-to-high load conditions (**Figure 12C,D**). Further explanation can be found elsewhere (Yousefi et al., 2019).

Figure 12 shows the unburned methane emissions of the NDDF engine under different engine loads. As expected, methane emissions grow significantly with increasing %NGs under all examined engine load conditions. However, this growth becomes much smaller at BMEPs of 12.15 and 17.60 bar (**Figure 12C,D**). It is observed that advancing SODI significantly decreases unburned methane emissions of the NDDF engine at BMEPs of 4.05 and 8.10 bar. However, methane emissions have a different behavior under higher engine load conditions. Advancing

Figure 13 | CO_2 equivalent emissions of NDDF engine at BMEPs of 4.05, 8.10, 12.15, and 17.60 bars.

SODI increases unburned methane emissions at the engine load of 12.15 bar and %NGs of 25% and 90%. Unburned methane emissions drop at SODI of −15° ATDC and 90% NG. Furthermore, unburned methane is relatively flat at engine load of 12.15% and 75% NG. At the highest engine load (BMEP = 17.60 bar), methane emission increase is observed with advancing SODI, especially for 50% and 65% NG. An explanation of this is observation reported in Yousefi et al., (2019).

Figure 13 depicts CO_2 equivalent emissions at different NDDF engine load conditions. As shown in **Figure 13A**, increasing %NG increases CO_2 equivalent emissions at any given SODI for BMEP of 4.05 bar. This is mainly due to a

significant amount of unburned methane emissions under low engine load conditions. Advancing SODI significantly reduces CO_2 equivalent emissions of the NDDF engine at BMEP of 4.05 bar. However, advancing SODI does not affect CO_2 equivalent emissions of the diesel engine under a load of 4.05 bar. At this NDDF engine load (BMEP = 4.05 bar), the lowest CO_2 equivalent emissions are 740 g/kW·h, which occur at 75% NG and SODI = −26° ATDC. However, the lowest CO_2 equivalent emissions of the diesel engine are 711 g/kW h.

At an engine load of 8.10 bar (**Figure 13B**) and retarded diesel injection timings, CO_2 equivalent emissions first decrease and then increase with increasing %NG. This is the result of thermal

efficiency and unburned methane emissions. At retarded SODI, thermal efficiency increases when increasing %NG from 0% to 50%, which decreases CO_2 equivalent emissions. However, unburned methane emissions increase with %NG, which leads to an increase in CO_2 equivalent emissions. The effect of the former is more significant, which yields lower CO_2 equivalent emissions with increasing %NG at retarded SODI. However, under advanced SODI, CO_2 equivalent emissions decrease with increasing %NG. This is due to the fact that the SODI timing is very advanced, which allows longer time for natural gas and diesel fuel to mix before the start of combustion, which makes the combustion happen quickly around the TDC and hence significantly decreases unburned methane emissions and increases thermal efficiency. Advancing SODI from a late timing decreases CO_2 equivalent emissions at BMEP of 8.10 bar. However, CO_2 equivalent emissions increase with further advancing diesel injection timing as a result of a decrease in thermal efficiency (**Figure 10B**). At this NDDF engine load (BMEP = 8.10 bar), the lowest CO_2 equivalent emissions are 613 g/kW h, which occur at 90% NG and SODI = $-24°$ ATDC. This is almost 7% lower than the lowest CO_2 equivalent emissions of the diesel engine (659 g/kW h), which occur at SODI = $-22°$ ATDC.

Figures 13C,D show that increasing %NG significantly decreases CO_2 equivalent emissions of the NDDF engine under BMEPs of 12.15 and 17.60 bar. As shown in **Figures 10 and 12**, increasing %NG increases thermal efficiency and unburned methane emissions of the NDDF engine at BMEPs of 12.15 and 17.60 bar. However, its effect on thermal efficiency is more significant than methane emissions, which results in a significant decrease in CO_2 equivalent emissions. At NDDF engine load of 12.15 bar, the lowest CO_2 equivalent emissions are 571 g/kW·h, which occur at 90% NG and SODI = $-14°$ ATDC. This is almost 11.8% lower than the lowest CO_2 equivalent emissions of the diesel engine (648 g/kW·h). Moreover, at BMEP = 17.60 bar, the lowest CO_2 equivalent emissions of the NDDF engine are 571 g/kW·h, which occur at 90% NG and SODI = $-16°$ ATDC. This is almost 6.4% lower than the lowest CO_2 equivalent emissions of the diesel engine (610 g/kW·h).

CONCLUSIONS

An experimental study was conducted to examine the effect of %NG on the combustion performance and GHG emissions of the NDDF engine under low-to-high engine load conditions. A sweep of diesel injection timing was also tested under each operating conditions. A CFD model was also used to further explain the mechanisms behind the phenomena observed in the experiments. The main findings of this study are outlined below.

- The effect of %NG on combustion performance depends on the engine load. The PPRR increases and then drops with increasing %NG under all examined engine load conditions. Increasing %NG from 0% to 50% under low load conditions and from 0% to 75% at high load conditions increases the local equivalence ratio inside the ignition kernel, which indicates that more premixed natural gas–air mixture participates in reactions during the premixed combustion

stage. This results in an increased flame temperature, intense HRR, and higher PPRR right after ignition. However, increasing %NG beyond this range decreases local equivalence ratio inside the ignition kernel, which leads to slower heat release and lower PPRR.

- Under low-to-medium load conditions, increasing %NG retards the combustion phasing at a given SODI. Under low-to-medium load conditions, the equivalence ratio of natural gas–air mixture and charge temperature around the ignition pocket is very low. These conditions cause flame quenching after the elapse of premixed and diffusion combustion stages, which, in turn, retards combustion phasing. However, under medium-to-high load conditions, the premixed equivalence ratio and charge temperature are high enough to support flame propagation. Therefore, increasing %NG increases flame propagation speed and generally advances the combustion phasing.

- Increasing %NG at retarded SODI significantly decreases the engine thermal efficiency under low-to-medium load conditions. However, advancing SODI significantly enhances thermal efficiency of the NDDF engine, especially at higher %NGs. Increasing %NG significantly increases thermal efficiency of the NDDF engine at medium-to-high load conditions due to improved flame propagation speed of the premixed natural gas–air mixture.

- Methane emissions grow significantly with increasing %NG under all examined engine load conditions. However, this growth becomes much weaker under medium-to-high engine load conditions. Increasing %NG significantly increases CO_2 equivalent emissions under engine low load conditions. This is due mainly to a significant amount of emitted unburned methane at low load conditions. However, increasing %NG significantly decreases CO_2 equivalent emissions of the NDDF engine by 6%–11% under medium-to-high load conditions.

DATA AVAILABILITY STATEMENT

The raw data supporting the conclusions of this article will be made available by the authors, without undue reservation.

AUTHOR CONTRIBUTIONS

AY wrote the manuscript with support from HG and MB. AY performed the numerical simulations and analyzed the experimental and numerical results. HG carried out the experiments. All authors provided critical feedback and helped shape the research, analysis and manuscript. MB supervised the project.

FUNDING

3B03.003) and National Research Council Canada through the internal Bioenergy Program. The numerical simulation was supported by CONVERGENT Science, Inc. and Compute Canada at the University of Manitoba.

REFERENCES

Ahmad, Z., Aryal, J., Ranta, O., Kaario, O., Vuorinen, V., and Larmi, M. (2018). An optical characterization of dual-fuel combustion in a heavy-duty diesel engine. SAE International, Technical Paper 2018-01–0252. https://doi.org/10.4271/2018-01-0252. Abstract.

Bataille, C., Sawyer, D., and Melton, N. (2015). Pathways to deep decarbonization in Canada. Carbon Management Canada, Low Carbon Pathways Group, SDSN-IDDRI.

Cesar, J., Egúsquiza, C., and Braga, S. L. (2015). Experimental investigation of a diesel cycle engine operating on natural gas/diesel dual-fuel mode. SAE International, Technical Paper 2011-36-0351. https://doi.org/10.4271/2011-36-0351.

Dahodwala, M., Joshi, S., Koehler, E. W., and Frank, M. (2014). Investigation of diesel and CNG combustion in a dual fuel regime and as an enabler to achieve RCCI combustion. SAE International, Technical Paper 2014-01-1308. https://doi.org/10.4271/2014-01-1308.

Guo, H., and Liko, B. (2019). "Injector tip temperature and combustion performance of a natural gas-diesel dual fuel engine at medium and high load conditions," in Proceeding of ASME 2018, V001T03A021. Available at: https://doi.org/10.1115/icef2018-9664.

Guo, H., Liko, B., Luque, L., and Littlejohns, J. (2017). "Combustion performance and unburned hydrocarbon emissions of a natural gas-diesel dual fuel engine at a low load condition," in Proceedings of the ASME 2017 internal combustion engine division fall technical conference ICEF2017, Seattle, WA, October 15–18, 2017, 1–9.

Guo, H., Neill, W. S., and Liko, B. (2015). "An experimental investigation on the combustion and emissions performance of a natural gas - diesel dual fuel engine at low and medium loads," in Proceedings of the ASME 2015 internal combustion engine division fall technical conference ICEF2015, Houston, TX, November 8–11, 2015, 130–137. https://doi.org/10.1115/ICEF2015-1041.

Jiaqiang, E., Pham, M. H., Deng, Y., Nguyen, T., Duy, V. N., Le, D. H., et al. (2018). Effects of injection timing and injection pressure on performance and exhaust emissions of a common rail diesel engine fueled by various concentrations of fish-oil biodiesel blends. Energy. 149, 979–989. doi:10.1016/j.energy.2018.02.053

Jupudi, R. S., Finney, C. E. A., Primus, R., Wijeyakulasuriya, S., Klingbeil, A. E., Tamma, B., et al. (2016). Application of high performance computing for simulating cycle-to-cycle variation in dual-fuel combustion engines. SAE International, Technical Paper 2016-01-0798. https://doi.org/10.4271/2016-01-0798.

Lounici, M. S., Loubar, K., Tarabet, L., Balistrou, M., Niculescu, D. C., and Tazerout, M. (2014). Towards improvement of natural gas-diesel dual fuel mode: an experimental investigation on performance and exhaust emissions. Energy. 64, 200–211. doi:10.1016/j.energy.2013.10.091

Mattson, J. M. S., Langness, C., and Depcik, C. (2018). An analysis of dual-fuel combustion of diesel with compressed natural gas in a single-cylinder engine. SAE International, Technical Paper 2018-01-0248. https://doi.org/10.4271/2018-01-0248.

Nithyanandan, K., Zhang, J., Li, Y., Meng, X., Donahue, R., Lee, C.-F., et al. (2016). Diesel-like efficiency using compressed natural gas/diesel dual-fuel combustion. J. Energy Resour. Technol. 138 (5), 052201. doi:10.1115/1.4032621

Papagiannakis, R. G., and Hountalas, D. T. (2004). Combustion and exhaust emission characteristics of a dual fuel compression ignition engine operated with pilot diesel fuel and natural gas. Energy Convers. Manag. 45 (18–19), 2971–2987. doi:10.1016/j.enconman.2004.01.013

Rahimi, A, Fatehifar, E., and Khoshbakhti Saray, R. (2010). Development of an optimized chemical kinetic mechanism for homogeneous charge compression ignition combustion of a fuel blend of n-heptane and natural gas using a genetic algorithm. Proc. Inst. Mech. Eng. Part D J. Automob. Eng. 224, 1141–1159. doi:10.1243/09544070JAUTO1343.

Richards, K. J., Senecal, P. K., and Pomraning, E. (2017). Converge 2.4 Manual, Madison, WI: Convergent Science, Inc.

Rochussen, J., and Kirchen, P. (2018). Characterization of reaction zone growth in an optically accessible heavy-duty diesel/methane dual-fuel engine. Int. J. Engine Res. 20, 483–500. doi:10.1177/1468087418756538.

Senecal, P. K., Richards, K. J., Pomraning, E., Yang, T., Dai, M. Z., McDavid, R. M., et al. (2007). A new parallel cut-cell cartesian CFD code for rapid grid generation applied to in-cylinder diesel engine simulations. SAE International, Technical Paper 2007-01-0159. doi:10.4271/2007-01-0159

Shim, E., Park, H., and Bae, C. (2018). Intake air strategy for low HC and CO emissions in dual-fuel (CNG-Diesel) premixed charge compression ignition engine. Appl. Energy. 225, 1068–1077. doi:10.1016/j.apenergy.2018.05.060

Song, H., Liu, C., Li, Y., Wang, Z., Chen, L., He, X., et al. (2018). An exploration of utilizing low-pressure diesel injection for natural gas dual-fuel low-temperature combustion. Energy. 153, 248–255. doi:10.1016/j.energy.2018.04.041

Tablan, A. D. (2014). "Diesel and compressed natural gas dual fuel engine operating envelope for heavy duty application andrew," in Proceedings of the ASME 2014 internal combustion engine division fall technical conference ICEF2014, Columbus, IN, October 19–22, 2014, 1–10.

Treasury Board of Canada Secretariat" (2017). Goverment of Canada. Https://Www.Canada.ca.

Wijeyakulasuriya, S. (2015). "Multidimensional modeling and validation of dual-fuel combustion in a large bore medium speed diesel engine," in Proceedings of the ASME 2015 internal combustion engine division fall technical conference ICEF2015, Houston, TX, November 8–11, 2015, 1–14.

Yousefi, A., and Birouk, M. (2016). Fuel suitability for homogeneous charge compression ignition combustion. Energy Convers. Manag. 119, 304–315. doi:10.1016/j.enconman.2016.04.056

Yousefi, A., and Birouk, M. (2017). Investigation of natural gas energy fraction and injection timing on the performance and emissions of a dual-fuel engine with pre-combustion chamber under low engine load. Appl. Energy. 189, 492–505. doi:10.1016/j.apenergy.2016.12.046

Yousefi, A., Birouk, M., and Guo, H. (2017). An experimental and numerical study of the effect of diesel injection timing on natural gas/diesel dual-fuel combustion at low load. Fuel. 203, 642–657. doi:10.1016/j.fuel.2017.05.009

Yousefi, A., Birouk, M., and Guo, H. (2019). Effect of diesel injection timing on the combustion of natural gas/diesel dual-fuel engine at low-high load and low-high speed conditions. Fuel. 235, 838–846. doi:10.1016/j.fuel.2017.05.009

Yousefi, A., Birouk, M., Lawler, B., and Gharehghani, A. (2015). Performance and emissions of a dual-fuel pilot diesel ignition engine operating on various premixed fuels. Energy Convers. Manag. 106, 322–336. doi:10.1016/j.enconman.2015.09.056

Yousefi, A., Guo, H., and Birouk, M. (2018). Effect of swirl ratio on NG/diesel dual-fuel combustion at low to high engine load conditions Appl. Energy. 229, 375–388. doi:10.1016/j.apenergy.2018.08.017

Yousefi, A., Guo, H., Birouk, M., and Liko, B. (2019). On greenhouse gas emissions and thermal efficiency of natural gas/diesel dual-fuel engine at low load conditions: coupled effect of injector rail pressure and split injection. Appl. Energy. 242, 216–231. doi:10.1016/j.apenergy.2019.03.093

Zheng, J., Wang, J., Zhao, Z., Wang, D., and Huang, Z. (2019). Effect of equivalence ratio on combustion and emissions of a dual-fuel natural gas engine ignited with diesel. Appl. Therm. Eng. 146, 738–751. doi:10.1016/j.applthermaleng.2018.10.045